scientific reports

Check for updates

OPEN

GYY4137 ameliorates blood brain barrier damage by inhibiting autophagy mediated occludin degradation in cardiac arrest and resuscitation

Pengyu Duan[1,3], Xiaoyan Li[1,3], Yonghong Bi[1,3], Weiyu Feng[1,3], Zhehao Jin[1,3], Xiaoqian Zhang[1,3], Guanghui He[1,3], Da An[2], Zhibin Wen[2] & Bing Zhang[1,3]✉

Cardiopulmonary resuscitation (CPR) after cardiac arrest (CA) is an important cause of neurological impairment and leads to considerable morbidity and mortality. The stability of the blood-brain barrier (BBB) is crucial for minimizing secondary neurological damage and improving long-term prognosis. However, the precise mechanisms and regulatory pathways that contribute to BBB dysfunction after CPR remain elusive. GYY4137 is an innovative hydrogen sulfide slow-release agent with excellent properties as a hydrogen sulfide substitute. The aim of this study was to investigate the protective effects of GYY4137 on CA/CPR and the underlying mechanisms of BBB protection. The effects of GYY4137 on systemic inflammation, BBB integrity, and autophagy were evaluated using a mouse CA/CPR model. The underlying mechanisms of occludin changes associated with GYY4137 were investigated using oxygen-glucose deprivation / reoxygenation (OGD/R) model. ELISA, neurological function and other tests showed that GYY4137 ameliorates systemic inflammation and neurological prognosis. Western blotting, transwell migration and tube formation assays showed that GYY4137 improves BBB function both in vivo and in vitro. The detection of autophagy flow and protein degradation pathways showed the inhibition of occludin reduction by GYY4137 was mainly achieved by suppressing autophagy mediated degradation. Taken together, GYY4137 may improve BBB dysfunction following CPR by increasing occludin content. This effect was achieved by inhibiting autophagic degradation rather than promoting synthesis. GYY4137 also mitigated systemic inflammation and improved neurological outcomes after CA/CPR. In summary, our study provides valuable insights into protecting the integrity of BBB and improving neurological outcomes after CPR.

Keywords Autophagy mediated degradation, Blood-brain barrier, Cardiac arrest and resuscitation, GYY4137, Occludin

Cardiopulmonary resuscitation (CPR) after cardiac arrest (CA) is the most urgent and dangerous situation frequently encountered in the clinic, and it is also one of the major challenges for clinicians. Despite some advances in CPR research and training that have improved the success rate of autonomic circulation restoration after initial resuscitation, the incidence of secondary neurological impairment remains as a pressing global problem[1–3]. Notably, disruption of the BBB is not only a precursor and frequent primary injury event, but also a consequence of central nervous system (CNS) disorders, as this disruption may promote the infiltration of leukocytes into the CNS, thereby amplifying lesion progression[4]. Previous studies have suggested that degradation of tight junction-associated proteins in the BBB after CPR may lead to impaired neurological function[5,6]. Suppression of protein degradation of key BBB components after CPR maintains the stability of the BBB function and may significantly influence neurological dysfunction after ischemia reperfusion injury[7,8].

[1]Department of Anesthesiology, Second Affiliated Hospital of Harbin Medical University, 246 Xuefu Road, Nangang District, Harbin 150086, Heilongjiang Province, China. [2]Department of Anesthesiology, First Affiliated Hospital of Harbin Medical University, Harbin, Heilongjiang Province, China. [3]The Key Laboratory of Anesthesiology and Intensive Care Research of Heilongjiang Province, Harbin, China. ✉email: 600771@hrbmu.edu.cn

Hydrogen sulfide (H_2S) is an important gaseous transmitter molecule in living organisms and the third gasotransmitter discovered so far. Numerous investigations have revealed the physiological regulatory functions of H_2S in various organs, including inhibiting inflammation, mediating autophagy, improving oxidative stress injuries, promoting angiogenesis, and inducing neutrophil apoptosis[9]. Within the CNS, H_2S can easily traverses the BBB without assistance and effectively penetrate cell membranes to execute its corresponding functions, which brings significant advantages for the treatment of CNS diseases[10]. Previous studies have shown that H_2S has a protective effect on neurological function after CPR, protects the structure and function of the BBB, and elevates tight junction proteins[6], but the exact mechanism of how H_2S regulates tight junction proteins is still unclear.

Autophagy is an evolutionarily conserved lysosomal degradation pathway triggered by various pathological processes, including organelle elimination and proteolysis[11]. Previous studies have shown that autophagy plays an important role in the progression of ischemia-reperfusion injury, affecting different kinds of neurons, microglia, astrocytes, and BBB[12,13]. In the BBB-related studies, on the one hand, autophagy could protect BBB by metabolizing damaged organelles and misfolded proteins; on the other hand, excessive activation of autophagy may further aggravate the structural damage and dysfunction of BBB[14,15]. Previous studies have shown that H_2S can inhibit autophagy[16–18], but the effect and mechanism of H_2S on regulation autophagy in BBB structure after CPR are not known.

In this study, we investigated the potential protective effects of an innovative H_2S donor GYY4137[19,20], including its effects on autophagy, systemic inflammation, neurological deficits, BBB permeability and tight junction proteins after CPR and related mechanisms.

Materials and methods

Animals

All experimental procedures were approved by the Institutional Animal Care and Use Committee of Harbin Medical University (Heilongjiang, China). Experimental animals were procured from the Animal Experiment Center at the Second Affiliated Hospital of Harbin Medical University. Animals were used and treated according to the guidelines of the Laboratory Animal Center of Harbin Medical University in this study. All studies involving animals are reported in accordance with the ARRIVE guidelines for reporting experiments involving animals[21,22].

Reagents

GYY4137 (GYY, a dichloromethane-free, water-soluble sodium salt form of the slow-releasing H_2S donor) and chloroquine (CQ) were purchased from Sigma-Aldrich (USA). Rapamycin (Rapa) was purchased from Solarbio (Bei Jing, China). (R)-MG-132 (MG-132, a proteasome inhibitor, the enantiomer of MG-132) and cycloheximide (CHX, a protein synthesis inhibitor) were purchased from MedChemExpress (USA).

Animal grouping and cardiac arrest / resuscitation model in mice

Male C57BL/6 mice weighing 25–28 g and 6–8 weeks old were randomized into different groups: Sham group (only oral catheterization and external jugular vein puncture and catheterization), CA/CPR group (CA/CPR procedure), CA/CPR + GYY group (intraperitoneal injection of GYY4137 4 mg/kg 1 h after CA/CPR), CA/CPR + Rapa group (intraperitoneal injection of rapamycin (3 mg/kg) after CA/CPR). In our preliminary experiment, we evaluated various dosages of GYY4137 to determine the most appropriate dose (Supplementary Fig. 1). Based on the evaluation results, we chose 4 mg/kg of GYY4137 and administered intraperitoneal injection to the CA/CPR + GYY group 1 h after CA/CPR.

CA and resuscitation model in mice were established as previously described[23,24]. Briefly, after anesthetized with sevoflurane, 50 ul (0.5 M) ice potassium chloride was injected to induce CA and the mice were removed from the ventilator. CPR was performed 6 min after CA, the ventilator was connected, $FiO_2 = 1.0$, intravenous injection of epinephrine 0.5-1.0 ml (16 mg/ml), and external chest compressions 300 times/min were performed until the return of spontaneous circulation (ROSC). If the duration of CPR exceeded 15 min without ROSC, CPR would be stopped. One hour after ROSC and recovery of spontaneous respiration, mechanical ventilation was stopped, the tracheal catheter and arteriovenous puncture catheter were removed, and then transferred to animal intensive care unit. The timeline of the animal experiment was shown in Supplementary Fig. 2.

Measurement of serum parameters

Serum levels of CRP, TNF-α, IL-18, IL-6, and IL-1β were measured using ELISA kits (Jingmei, China) according to the manufacturer's instructions. Twenty-four hours after CPR, mice blood was collected and centrifuged for 15 min (3000 g).

Evaluation of neurological function and overall survival rate

The general neurological performance was assessed at 1 d, 3 d, and 7 d after ROSC by one investigator who was blinded to the groups using the neurological deficit scores (NDS), which was established in mice undergoing CA[24]. The score ranges from 12 points indicating normal function to 0 representing brain death. Survival rate was evaluated during the 14 days after ROSC.

Novel object recognition (NOR)

The Novel Object Recognition test (NOR) was carried out at 7 d after ROSC as previous reported[25,26]. The mice were acclimated in the laboratory for five days before the test. Then, the mice were allowed to explore freely in an empty box (50 × 50 × 50 cm) for 10 min. After 24 h, the mice were placed in the same box in which two identical

objects were placed and allowed to explore for 10 min. After an hour, the mice were placed in the same box and one of the two objects was replaced with a new object. The mice were allowed to explore for five minutes to test. For analysis, the recognition (or preference) index was calculated as the ratio of the time spent exploring the new objects to the total time spent exploring the new and familiar objects.

Neuronal counts

After 14 days of ROSC, the survival neurons in hippocampal CA1 region was investigated. Mice were deeply anesthetized with sevoflurane and perfused with 5 ml 0.1 mol/l phosphate buffered saline and 4% paraformaldehyde through the heart. Hippocampal tissue were removed quickly and fixed in 4% paraformaldehyde before paraffin embedding. Hematoxylin and eosin (H&E) - stained sections of the hippocampus were examined. Viable neurons were defined as cells with a distinct nucleus and nucleolus, while ischemic neurons were recognized by the pyknotic or karyorrhectic nuclei lacking a clear nucleolus. An observer who was blinded to the experimental protocol counted the numbers of pyramidal neurons in high-power field (× 400). The number of neurons in the hippocampal CA1 region was quantitated as the average of three sections per mouse. In each section, the number of neurons was averaged from three random different fields of view in the CA1 region[27].

Assessment of brain water content

Brain tissue was immediately dissected, weighed, and defined as the wet weight at 24 h after ROSC. Tissues were then placed in an oven (105 °C) and dried for 72 h to obtain the dry weight. The water content was calculated by the formula: ([wet weight – dry weight] / wet weight) × 100%[28].

Evans blue leakage

Twenty-four hours after ROSC, 2% Evans blue (EB; Sigma, USA) was administered intravenously and circulated for one hour. Then, mice were perfused intracardially with saline to remove residual EB. To quantitatively measure EB leakage, the cerebral cortex was homogenized in 1 ml of trichloroacetic acid and then centrifuged at 12 000 g for 20 min. The concentration of EB extracted in the supernatant was analyzed spectrophotometrically at 620 nm[29].

Transmission electron microscopy (TEM)

The anesthetized mice were perfused with 0.9% saline, and 1 mm^3 cerebral cortex tissue blocks were taken at 24 h after ROSC. Next, the fresh tissue blocks were put into 2.5% glutaraldehyde for TEM (Solarbio) at 4 ℃ for 4 h and then fixed with 1% osmium tetroxide buffer for 2 h at room temperature, followed by dehydration with gradient alcohol. Subsequently, the sections were embedded and cut into ultrathin sections (60 nm). Finally, the ultrastructure of tight junction was observed using a transmission electron microscope (HITACHI, HT7700, Japan).

Cerebral microvessel isolation

The brain microvessels were isolated as previously described with minor adjustments[30,31]. After processing the CA/CPR model for 24 h, the cerebellum and olfactory bulb were removed, the remaining brain was rapidly homogenized in 3 ml of cold sucrose buffer (0.32 M sucrose, 5 mM HEPES, pH 7.4). Then, the brain homogenate was centrifuged at 1000 g for 10 min. The supernatant containing most of the neuronal components and dense white myelin sheath layer at the top of the particles was discarded. Next, the pellets were resuspended in 3 ml sucrose buffer and centrifuged at 1000 g for 10 min to remove any remaining myelin sheaths. The 40 g spin was used to separate the large blood vessels from capillaries. Finally, wash the remaining particles four times with 1 ml sucrose buffer, and centrifuge at 350 g for 10 min to obtain the final microvascular precipitate.

Cell culture and oxygen-glucose deprivation / reoxygenation model

The mouse brain microvascular endothelial cells bEnd.3 was purchased from Procell Life Science & Technology Co., Ltd (Wu Han, China) and cultured in Dulbecco's modified Eagle's medium (Gibco, USA) supplemented with 10% fetal bovine serum (Adamas, China), 100 U/ml penicillin and 100 mg/ml streptomycin (New Cell & Molecular Biotech, China) at 37 °C in a 5% CO_2 humidified incubator.

Oxygen-glucose deprivation / reoxygenation (OGD/R) was reproduced in vitro as reported previously[32]. The bEnd.3 cells were placed in a 37 °C anaerobic chamber (5% CO_2, 95% N_2) and cultured in glucose-free medium for 4 h. After the OGD, the cells were placed in glucose-containing DMEM with 10% FBS and then incubated under normoxic conditions for 12 h. Control samples were taken from cells cultured under normal conditions. The OGD/R + GYY, OGD/R + CHX, OGD/R + CHX + GYY, OGD/R + MG, OGD/R + CQ and OGD/R + GYY + Rapa groups were treated with GYY4137 (50 μM), cycloheximide (20 μg/ml), cycloheximide (20 μg/ml) + GYY4137 (50 μM), MG-132 (5 μM), chloroquine (10 μM), GYY4137 (50 μM) + rapamycin (5 ug/ml) respectively during the reoxygenation period.

Cell viability assay

Cell viability was detected using the Cell Counting Kit-8 (CCK-8) assay kit (New Cell & Molecular Biotech, China). The bEnd.3 cells were seeded on 96-well plates at a density of 5×10^3 cells per well and incubated overnight. After the OGD/R model establishment and treat with GYY4137 (10 μM, 50 μM, 100 μM), 10 μl CCK-8 reagent was added into 100 μl culture medium per well and incubated for 1 h. Optical density (OD) value was measured at 450 nm.

RFP-mWasabi-LC3 staining

The RFP-mWasabi-LC3 lentivirus was purchased from Genechem (Shanghai, China). The stably transfected bEnd.3 cells were cultured according to the manufacturer's instructions. After the OGD/R model establishment and treat with GYY4137, the cells were viewed under a fluorescence microscope. Green dots indicate autophagosomes and red dots indicate autophagosomes and autolysosomes. Yellow dots resulting from the merging of the red and green channels indicate autophagosomes, while red dots not overlapping with green dots indicate autolysosomes. The number of mWasabi and RFP dots was determined by manual counting of the fluorescent dots in five high-power fields (400 ×, Invitrogen).

In vitro BBB model

The bEnd.3 cells were seeded onto the transwell membrane (0.4 mm pore, 11 mm diameter; Corning) at a density of 2×10^4 cells. Cultures were maintained for four days to reach confluence. To assess paracellular permeability, FITC-dextran (40 kDa; Sigma, USA) was added into the luminal chamber at a concentration of 1 μM in 400 μl medium. Fluorescence intensity was measured one hour later using 100 μl medium from the lower chamber. The diffusion rate of tracers from the luminal to the abluminal chamber was determined and expressed as $pmol{\cdot}mm^2{\cdot}min^{-1}$.

Transwell migration assays

For cell migration assays, 5×10^4 cells suspended in medium without serum were seeded in the upper chamber (BD Biosciences, USA)[33]. Then, 600 μl medium with 10% FBS was added into the lower chamber. After 24 h, cells on the top surface were removed and the underside of the membrane was fixed in 4% paraformaldehyde for 30 min and stained with 0.1% crystal violet. Then, cells were quantified under a microscope (100 ×).

Tube formation assay

For the tube formation assay, 96-well plates were coated with 50 μl/well Matrigel (Corning, USA) and incubated to polymerize for 1 h. Cells were re-seeded in Matrigel matrix-coated plates (3×10^4 cells/well) for 4 h. Tubular structures were photographed using a microscope (100 ×), and quantified by measuring the total tube length with ImageJ software.

Western blotting

Western blotting was performed as previously described[34]. In brief, 24 h after ROSC, cerebral microvessels, cerebral cortex, or cells were homogenized in protein lysis buffer containing protease inhibitors (Beyotime, China) and phosphatase inhibitors (Roche, China), and debris was removed by centrifugation. Samples were resolved on polyacrylamide sodium dodecyl sulfate gels and electrophoretically transferred to polyvinylidene difluoride membranes. Membranes were blocked with 5% skim milk and incubated with primary antibodies against Occludin (Proteintech Group), Claudin-5 (Wanleibio), ZO-1 (Proteintech Group), LC3B II/I (CST), ATG5 (Proteintech Group), p62 (CST), Albumin (Wanleibio) and horse-radish peroxidase-conjugated secondary antibodies (1 : 2000, ZSGB-BIO). The dilution of the above primary antibodies was 1 : 1000. Protein bands were visualized using the highly sensitive ECL detection reagents. β-actin (1:2000, Santa Cruz, USA) was used as the protein control.

Real-time polymerase chain reaction analysis

Real-time quantitative polymerase chain reaction was used to analyze the mRNA levels of Occludin, Claudin-5 and ZO-1 in cerebral microvessels and cells at 24 h after ROSC[35]. Total RNA was extracted using an RNA Extraction Kit (Invitrogen, USA) and converted to first-strand cDNA according to the manufacturer's instructions (Toyobo, China). Real-time PCR was performed using a SYBR® Prime-Script™ RT-PCR Kit in a LightCycler System (Roche Diagnostics, UK). The primer sequences were designed by Primer 5.0 and purchased from Invitrogen. The following are PCR primer sequences: Occludin (*Ocln*): sense, 5′-AAGTCAACACCTC TGGTGCC-3′ and anti-sense, 5′-TTCCTGCTTTCCCCTTCGTG-3′; Claudin-5 (*Cldn5*): sense, 5′-CATCGT TGTCCGCGAGTTCT-3′ and antisense, 5′-ACTTGACCGGGAAGCTGAAC-3′; ZO-1 (*Tjp1*): sense, 5′-CG GCCGCTAAGAGCACAG-3′ and antisense, 5′-CTTCAGCTGGCCCTCCTTTT-3′; *β-actin*: sense, 5′-GGAC CTGACAGACTACCTCAT-3′ and antisense, 5′-GCTCGAAGTCTAGAGCAACATAG-3′. Amplification was performed with the cycles: 95 °C for 30 s, followed by 40 cycles of denaturing at 95 °C for 5 s and annealing at 60 °C for 20 s. All reactions were performed in triplicate. Data analysis was performed using the $2^{-\triangle\triangle CT}$ method, β-actin was used as the reference gene.

Statistical analysis

Data are presented as mean ± SD or median (interquartile range) and were analyzed using SPSS 28.0 for Windows (SPSS Inc., Chicago, IL). The Shapiro-Wilk normality test was used to test the normality of the continuous data. One-way analysis of variance (ANOVA) followed by Bonferroni's test was used for multiple comparison when data satisfied for normal distribution and homogeneity of variance. The data with a non-normal distribution were analyzed by Kruskal-Wallis and Mann-Whitney U test. Kaplan-Meier survival curves were compared using the log-rank test. $P<0.05$ was considered statistically significant.

Results

GYY4137 ameliorated systemic inflammation and neurological prognosis after cardiac arrest and resuscitation

To investigate the effect of GYY4137 on systemic inflammation, ELISA was used to evaluate inflammatory factors, including CRP, TNF-α, IL-18, IL-6, and IL-1β in the serum of mice. As depicted in Fig. 1A, 24 h after CA/

CPR, the levels of inflammatory factors in the serum of the CA/CPR group were significantly higher than those of the Sham group. Notably, the levels of these factors in the CA/CPR + GYY group were reduced, indicating a suppressive effect on the inflammation. To elucidate the effect of GYY4137 on the neurological function in CPR mice, a comprehensive assessment involving neurological scoring, NOR experiments, and histological examination of neurons in the hippocampal CA1 region were conducted. As shown in Fig. 1B, on the first day following CA/CPR, the neurological scores of the CA/CPR group significantly decreased compared with the Sham group. Conversely, the CA/CPR + GYY group demonstrated substantial improvement in NDS compared with the CA/CPR group. However, on days 3 and 7 after resuscitation, both the CA/CPR group and CA/CPR + GYY group exhibited decreased NDS compared with the Sham group, with no significant differences between the two groups. On the seventh day after resuscitation, NOR experiment was performed to assess cognitive memory function. As shown in Fig. 1C, the CA/CPR group and the CA/CPR + GYY group displayed reduced exploration time of novel objects in comparison to the Sham group. Remarkably, the CA/CPR + GYY group exhibited significantly increased exploration time compared with the CA/CPR group. In order to detect the potential effect of GYY4137 on the cognitive function after CA/CPR, H&E staining was performed in hippocampal CA1 region at the 14-day after CA/CPR. The neurons in the Sham group displayed orderly arrangement, whereas those in the CA/CPR group and CA/CPR + GYY group presented sparser arrangement and decreased counts, with unclear neuronal cell outlines that were counted and tallied. In Fig. 1D, quantitative analysis confirmed a substantial reduction in the neuron number in CA1 region in the CA/CPR group compared with the Sham group. The number of neurons in the CA/CPR + GYY group was significantly increased compared to the CA/CPR group. Furthermore, as shown in Fig. 1E, the survival rate at 14 days after CPR was decreased in both the CA/CPR and CA/CPR + GYY groups compared with the Sham group, while the survival rate was significantly increased in the CA/CPR + GYY group compared with the CA/CPR group. These results suggested that GYY4137 not only attenuated the systemic inflammation at the early stage after CA/CPR, but also improved the survival rate and neurological prognosis of mice.

GYY4137 improved BBB function at the early stage after CA/CPR

To evaluate the function of the BBB after CA/CPR, immunoblotting experiments were conducted on cerebral microvascular endothelial cell proteins at 24 h after CPR. The levels of tight junction proteins including occludin, claudin-5, and ZO-1 were evaluated (Fig. 2A and B). The levels of these tight junction proteins were significantly decreased in the CA/CPR group compared with the Sham group. However, tight junction proteins were significantly higher in the CA/CPR + GYY compared with the CA/CPR group. Tight junctions are critical functional units for maintaining BBB permeability. Therefore, the TEM analysis was performed to investigate the ultrastructure of tight junctions in the cerebral cortex. As shown in Fig. 2D, the tight junctions in the CA/CPR group demonstrated a disorganized and diffuse structure with severe localized endothelial damage. However, the structure of tight junction was significantly improved with clarity and integrity after GYY4137 treatment. The relative mRNA expression of claudin-5 and ZO-1 was significantly reduced in the CA/CPR and CA/CPR + GYY groups compared with the Sham group. Impressively, the levels of mRNA expression of claudin-5 and ZO-1 were significantly increased in the CA/CPR + GYY group compared with the CA/CPR group. Interestingly, the mRNA expression of occludin remained relatively stable in all three groups (Fig. 2C). The function of BBB was further evaluated through EB leakage experiments at 24 h after resuscitation. The graphical representation of brain EB leakage (Fig. 2E) and the quantification of EB content (Fig. 2F) both indicated increased EB content in the CA/CPR group and CA/CPR + GYY group compared with the Sham group. However, compared with the CA/CPR group, the EB content was decreased in the CA/CRP + GYY group, indicating that GYY4137 alleviated BBB damage and EB leakage. Cerebral edema was also assessed by analyzing the dry-to-wet weight ratio of brain at one day after resuscitation. As shown in Fig. 2G, the brain water content was elevated in the CA/CPR group and CA/CPR + GYY group compared to the Sham group. However, compared with the CA/CPR group, those receiving GYY4137 treatment showed a significant decrease in brain water content, highlighting GYY4137's ability to reduce cerebral edema in the early stage after resuscitation. Albumin, which is usually not present in the brain, is another indicator of BBB function. One day following CA/CPR, albumin was detected in the mice brain (Fig. 2H and I). Compared with the CA/CPR group, the albumin levels in the CA/CRP + GYY group decreased, indicating that GYY4137 alleviated the leakage of albumin into the brain after CA/CPR. In summary, these findings collectively demonstrated that GYY4137 not only increased the content of tight junction proteins in the early stage after resuscitation, but also reduced cerebral edema and improved BBB function.

GYY4137 augmented the function of endothelial cell tight junctions after OGD/R

The viability of bEnd.3 cell after OGD/R was conducted using CCK-8 assay. Firstly, different concentrations of GYY4137 were administered to determine the most suitable concentration for subsequent experiments. As depicted in Fig. 3A, cell viability significantly decreased in all groups except the Control group. Compared with the OGD/R group, cell viability increased in both the OGD/*R* + 50 μM GYY group and the OGD/*R* + 100 μM GYY group. However, the difference between these two groups lacked statistical significance, so a concentration of 50 μM GYY4137 was chosen for subsequent experiments. Subsequently, we conducted immunoblotting experiments on BBB-related tight junction proteins to assess their content in endothelial cells (Fig. 3B and C). Compared with the control group, the levels of occludin, claudin-5, and ZO-1 proteins in the OGD/R and OGD/R + GYY groups were significantly reduced. Compared with the OGD/R group, the OGD/R + GYY group demonstrated a considerable increase. The barrier function of bEnd.3 cells was evaluated by dextran permeation assay (Fig. 3D). The leakage of FITC-dextran from the lower compartment was significantly increased in both the OGD/R group and the OGD/*R* + 50 μM GYY group compared with the Control group. However, dextran leakage was significantly improved in the OGD/*R* + 50 μM GYY group compared with the OGD/R group. The migratory ability was detected using the transwell assay (Fig. 3E and F). Compared with the Control group, the

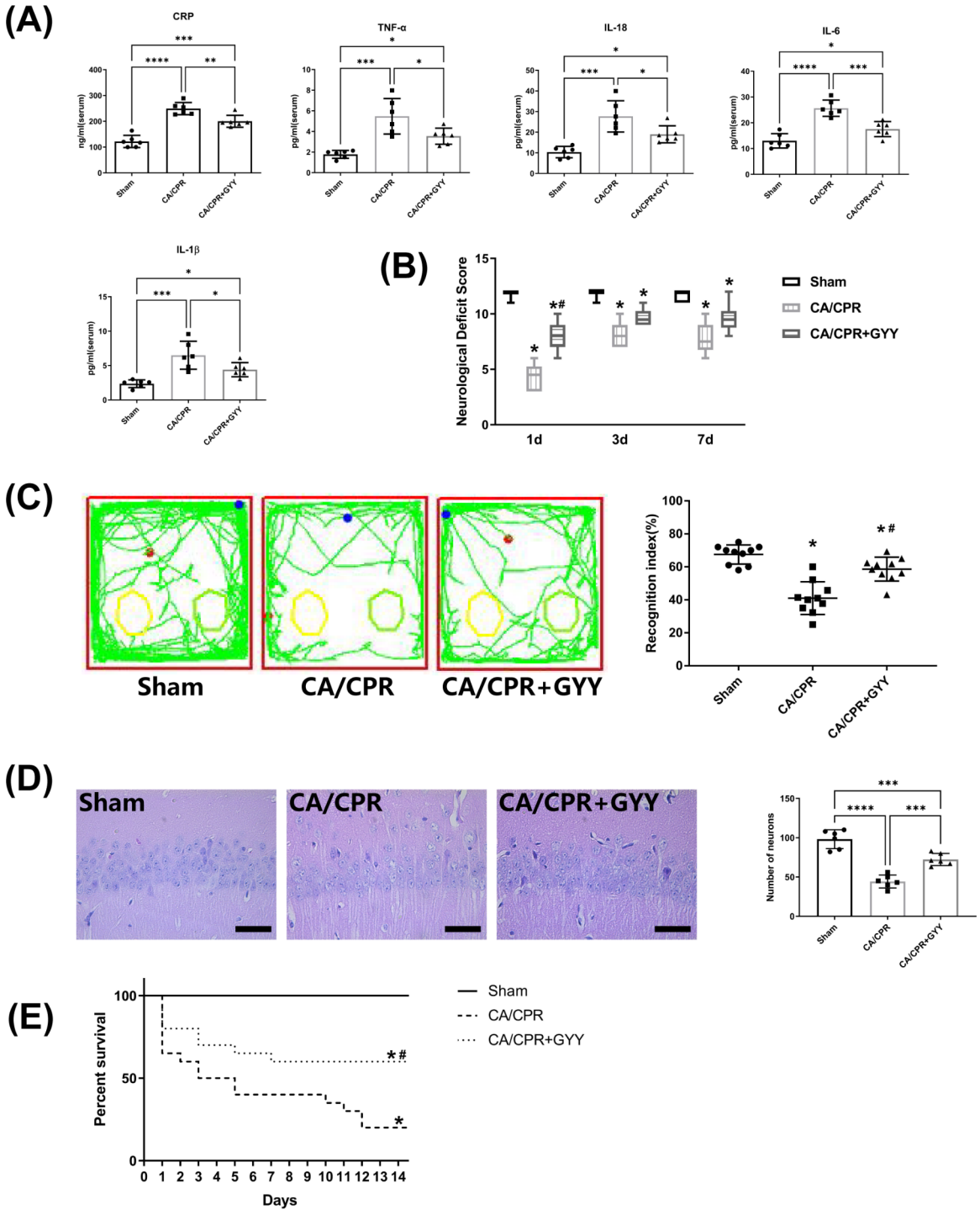

cell migration ability was significantly reduced in the OGD/R and OGD/R + GYY groups. Compared with the OGD/R group, the cell migration ability of the OGD/R + GYY group was greatly enhanced. The tube formation ability was assessed using the tube formation assays (Fig. 3G and H). Compared with the Control group, the total tube length in OGD/R group and OGD/R + GYY group was significantly reduced. Compared with OGD/R group, the total tube length in OGD/R + GYY group significantly increased. These results once again confirmed that GYY4137 improved BBB function by enhancing the extent of endothelial cell tight junctions in the in vitro OGD/R model.

◀**Fig. 1**. GYY4137 ameliorated systemic inflammation and neurological prognosis after cardiac arrest and resuscitation. (**A**) The levels of CRP, TNF-α, IL-18, IL-1β, and IL-6 in peripheral blood samples harvested from the mice subjected to Sham, CA/CPR, CA/CPR + GYY were spectrophotometrically measured. (**A**: CRP: $P < 0.0001$, F = 44.87; TNF-α: $P = 0.0002$, F = 16.44; IL-18: $P = 0.0002$, F = 16.52; IL-6: $P < 0.0001$, F = 28.07; IL-1β: $P = 0.0004$, F = 14.03). (**B**) Neurological deficit score at 1 d, 3 d and 7 d after ROSC. Scale 12 indicates a functionally normal; scale 0 represents brain death. (**B**: 1d: $P < 0.0001$, F = 142.2; 3d: $P < 0.0001$, F = 61.81 ; 7d: $P < 0.0001$, F = 28.36). (**C**) Representative motion trajectory (left) and the recognition index (right) of novel objection recognition at 7 d after ROSC. The green line represents the trajectory of the mice during the exploration period, indicating movement path. The yellow circle denotes familiar objects, while green circle indicates novel objects introduced during the testing phase. The red dot marks the initial position of the mouse at the beginning of the trial, and the blue dot represents the position of the mouse at the end of the trial. (**C**: $P < 0.0001$, F = 29.43). (**D**) Representative images (400 ×) of H&E staining in the CA1 region of mouse hippocampus (left) and the number of viable neurons in the CA1 region (right). Scale bar indicates 50 μm. (**D**: $P < 0.0001$, F = 48.13). (**E**) Survival rate after ROSC within 14 days. (**E**: $P < 0.0001$ Chi square = 26.90). The data are the means ± SD. $n \geq 3$. $^{\#}P < 0.05$ versus CA/CPR. $^{*}P < 0.05$; $^{**}P < 0.01$; $^{***}P < 0.001$; $^{****}P < 0.0001$.

GYY4137 inhibited autophagy in BBB endothelial cells in the early stage after resuscitation; and autophagy mediated the regulation of occludin protein content

In the early stage after CA/CPR in mice, GYY4137 showed a regulatory effect on endothelial cells within the BBB. GYY4137 not only constrained the intensity of autophagy, but also regulated occludin through the autophagy pathway, which has been confirmed both in vivo and in vitro. Specifically, GYY4137 not only augmented the content of occludin, but also exerted influence over autophagic process. The autophagy-associated markers including LC3B II, ATG5, and p62 were evaluated in Fig. 4. Compared with the Sham group, significant autophagy enhancement was observed in cerebral microvessels of the CA/CPR group. In contrast, the autophagy intensity showed a significant decrease in the CA/CPR + GYY group compared with the CA/CPR group (Fig. 4A and B). Similarly, in the in vitro experiment, a significant increase of autophagy intensity was observed in both the OGD/R and OGD/R + GYY groups compared with the Control group. Remarkably, the OGD/R + GYY group displayed a significant decrease in autophagy intensity compared with the OGD/R group (Fig. 4C and D). The RFP-mWasabi-LC3 staining can be used to localize and assess autophagic flux, which is not limited by pH changes in the cellular environment. Therefore, we generated a lentiviral vector carrying RFP-mWasabi-LC3 to assay autophagic flux, autophagosome biogenesis, maturation, and lysosomal degradation. As shown in Fig. 4E and F, both the mWasabi/RFP and RFP dots were significantly increased in the OGD/R and OGD/R + GYY groups, indicating the enhancement of autophagic flow. Treatment with GYY4137 decreased LC3 incorporation into autolysosomes but increased LC3 incorporation into autophagosomes. Clearly, these data demonstrated that treatment with GYY4137 reduced the accumulation of autolysosomes as well as inhibited autophagy at late stage, which may limit autophagy mediated protein degragation. These results collectively revealed that inhibition of autophagy by GYY4137 was associated with the subsequent increase in occludin protein levels.

To investigate whether the effect of GYY4137 on occludin acts through autophagic modulation, we performed the experimental design in Fig. 5. Rapamycin (Rapa) was used to enhance autophagy intensity, and the content of occludin were detected in the extracted brain microvessels. The results showed that, the levels of occludin were significantly decreased in the other three groups compared with Sham group. However, compared the CA/CPR group, the CA/CPR + GYY group demonstrated a marked increase in occludin content. Intriguingly, in the CA/CPR + Rapa group, autophagy was enhanced while the content of occludin in cerebral microvessels remained unchanged. This observation suggested that the enhancement of autophagy after CA/CPR did not significantly impact the occludin protein content in the cerebral microvessels (Fig. 5A and B). To evaluate BBB function, the quantification of EB and cerebral edema were conducted (Fig. 5C and D). Compared with CA/CPR group, the BBB function in the CA/CPR + Rapa group did not change significantly. Taken together, these data suggested that GYY4137 involved in the inhibition of autophagy in cerebral endothelial cells after CA/CPR in mice, concurrently leading to the augmentation of occludin.

Autophagy mediated protein degradation is the predominant mechanism behind the reduction of occludin following OGD/R

Based on the findings presented in figures above, it could be deduced that GYY4137 enhanced the protein levels of occludin, claudin-5, and ZO-1 in brain microvessels after CA/CPR. Moreover, at the mRNA level, GYY4137 was also confirmed to upregulate the mRNA of claudin-5 and ZO-1, which is consistent with changes in protein levels. Nevertheless, as illustrated in Fig. 2C, the occludin mRNA remained relatively unchanged in the Sham group, CA/CPR group, and CA/CPR + GYY group. This discrepancy between occludin protein and mRNA content could be attributed to potential fluctuations in both translation efficiency and protein degradation rate. To investigate whether the changes in occludin content were attributed to translation or degradation, the mRNA levels in endothelial cells were assessed in the in vitro experiments (Fig. 6A). Similar to the in vivo results, there was no significant difference in the relative expression of occludin mRNA among the Control group, OGD/R group, and OGD/R + GYY group. To discern whether alterations in mRNA translation influenced changes in protein content, we used a protein synthesis inhibitor CHX to block ribosome binding to mRNA. Results in Fig. 6B and C illustrated a substantial reduction in occludin protein in the OGD/R + CHX group compared with the OGD/R group, while occludin increased remarkably in the OGD/R + CHX + GYY group. Notably, the occludin within the OGD/R + CHX + GYY group surpassed that of the OGD/R + CHX group. This result suggested the impact of GYY4137 on occludin was not predominantly mediated through modulation of mRNA

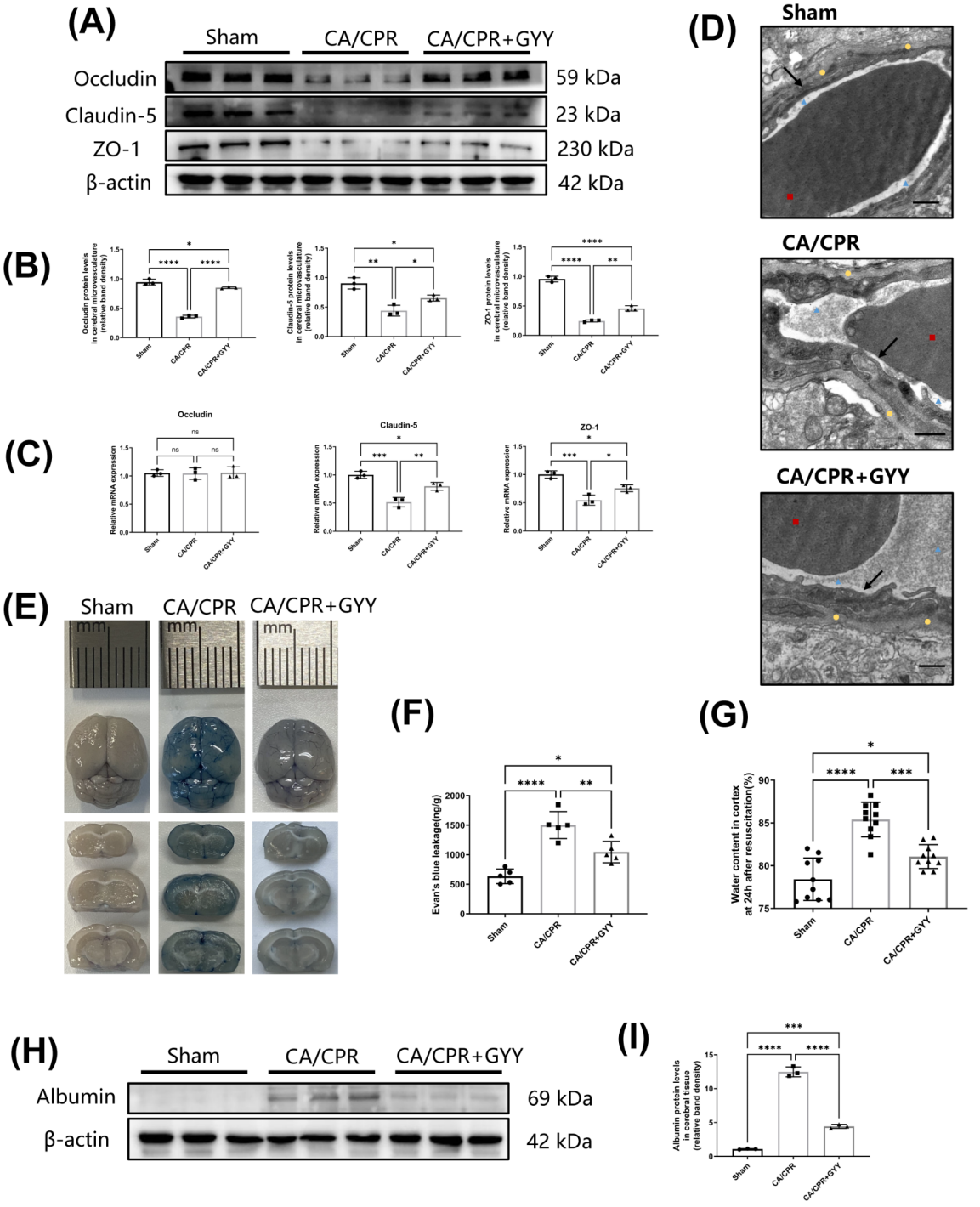

translation. Proteins are mainly degraded and replaced through two pathways, namely the ubiquitin-proteasome system and autophagy pathway. To investigate whether alterations in occludin after OGD/R were associated with the ubiquitin-proteasome system or autophagy pathway, the proteasome inhibitor MG-132 and autophagy inhibitor CQ were employed. Results depicted in Fig. 6D and E demonstrated that the OGD/R + MG group exhibited marginal alterations in occludin compared with the OGD/R group. In contrast, the OGD/R + CQ group exhibited significant increase in occludin content. This differences between the relative occludin mRNA content and protein content suggested the autophagy degradation pathway played an important regulatory role in this process. To further assess whether GYY4137 modulated occludin by influencing the autophagy degradation pathway, we validated this hypothesis in in vitro experiments (illustrated in Fig. 6F and G). The occludin protein content significantly decreased in OGD/R group, OGD/R + GYY group and OGD/R + GYY + Rapa group when compared with Control group. Occludin exhibited a significant increase in the OGD/R + GYY group compared

◀**Fig. 2**. GYY4137 improved BBB function at the early stage after CA/CPR. (**A**) Representative immunoblot images and (**B**) quantitation of occludin, claudin-5 and ZO-1 expression in cerebral microvessels of mice in Sham, CA/CPR, CA/CPR + GYY groups at 24 h after ROSC. β-actin was used as the protein loading control. The images of western blot data derived from triplicate blots conducted as three independent experiments. (**B**: occludin: $P < 0.0001$, F = 279.7; claudin-5: $P = 0.0014$, F = 23.62; ZO-1: $P < 0.0001$, F = 249.1). (**C**) Relative mRNA expression of occludin, claudin-5, ZO-1 in cerebral microvessels harvested from the mice described above. (**C**: occludin: $P = 0.9846$, F = 0.01559; claudin-5: $P = 0.0006$, F = 33.34; ZO-1: $P = 0.0008$, F = 28.88). (**D**) Representative electron micrographs showing the tight junction structure of BBB. The black arrow points to the tight junctions between endothelial cells, indicating the integrity of the BBB. The red square marks the location of a red blood cell within the capillary. The blue triangle represents the vascular lumen, while the yellow circle indicates the basement membrane surrounding the endothelial cells. Scale bar indicates 5 μm. (**E**) Representative brain images of EB leakage experiment and (**F**) BBB permeability evaluated using EB at 24 h after ROSC. (**F**: $P < 0.0001$, F = 27.91). (**G**) Brain water content of mice in Sham, CA/CPR, and CA/CPR + GYY groups at 24 h after ROSC. (**G**: $P < 0.0001$, F = 30.72). (**H**) Representative immunoblot images and (**I**) quantitation of albumin in cerebral cortex harvested from the mice described above. The images of western blot data derived from triplicate blots conducted as three independent experiments. (**I**: $P < 0.0001$, F = 496.6). The data are the means ± SD. $n \geq 3$. $^{*}P < 0.05$; $^{**}P < 0.01$; $^{***}P < 0.001$; $^{****}P < 0.0001$.

with the OGD/R group. However, in the OGD/R + GYY + Rapa group, although rapamycin enhanced autophagy, failed to exhibit a similar result of increased occludin content, highlighting that rapamycin-mediated autophagy enhancement diminished the protective effect of GYY4137 on occludin. Collectively, these in vitro and in vivo results suggest that the protective effect of GYY4137 on BBB following CA/CPR is mainly achieved by inhibiting autophagy mediated degradation of occludin protein.

Discussion

BBB plays an important role in maintenance of brain health, its function is closely related to various neurological diseases, including postoperative cognitive dysfunction, ischemic brain injury, and so on[36–40]. Previous studies have confirmed that H_2S could reduce the systemic inflammation, improve the prognosis of neurological function, and protect the BBB function after CA/CPR[41–43]. However, the specific regulatory mechanism is not yet clear. In this investigation, we found that GYY4137 could alleviate systemic inflammation, inhibit autophagy mediated degradation of occludin protein in the BBB, maintain BBB function, and improve long-term neurological prognosis after CA/CPR.

Several studies have confirmed that H_2S can exert autophagy regulation through multiple molecular mechanisms[16,18,44–46]. H_2S donors have been shown to reduce the upregulation of lactate dehydrogenase B induced by platelet-derived growth factor-BB (PDGF-BB), thereby diminishing the interaction between lactate dehydrogenase B and ATP6V1A (a key component of lysosomal acidification) and inhibiting autophagy[44]. In uremic cardiomyopathy and traumatic brain injury, H_2S donors activate the PI3K/AKT/mTOR signaling pathways to inhibit autophagy and protect cells[18,45]. In a ventilator-induced lung injury model, H_2S suppresses the PERK/eIF2α/ATF4/GADD34 pathway, thereby inhibiting autophagy[46]. In addition, in sleep deprivation animals, H_2S donor inhibits excessive autophagy in the hippocampus through a Sirt-1-dependent mechanism, leading to improved cognitive outcomes[16]. In our study, we demonstrated that GYY4137 reduced the inflammation, inhibited autophagy, and improved neurological outcomes after CA/CPR. These findings strongly support the role of GYY4137 in autophagy regulation, but the exact molecular pathway of its action remains to be explored further.

The BBB is an important biological interface formed primarily by brain microvascular endothelial cells with tight junctions and supported by astrocytes, pericytes, and perivascular microglia. Previous studies have demonstrated that disruption of BBB following CA/CPR is closely related to the decrease in occludin, claudin-5, and ZO-1, and that inhibition of the reduction of these tight junction proteins can improve BBB function[6,40]. In our study, we observed that GYY4137 consistently upregulated the protein and mRNA levels of claudin-5 and ZO-1, which is consistent with previous findings[47,48]. However, it is still unclear how GYY4137 regulates the transcription of Claudin-5 and ZO-1. It has been shown that in a mouse model of ethanol-induced cerebral microvascular endothelium injury (bEnd.3), H_2S reduce the methylation of CpG islands in the promoter of ZO-1, thereby enhancing its mRNA expression; however, such an effect was not observed for claudin-5, suggesting that there may be different regulatory mechanisms of H_2S on ZO-1 and Claudin-5[49]. We speculate that GYY4137, which acts as an H_2S donor, may also regulate Claudin-5 and ZO-1 transcription through epigenetic modifications. An interesting result in this experiment is that GYY4137 increased the protein content of occludin without a corresponding rise in its mRNA levels, indicating that the upregulation of occludin protein may be mediated through mechanisms other than transcription. Therefore, the mechanisms of GYY4137 regulation of ZO-1, claudin-5 and occludin after CA/CPR are complex and not identical, and the exact mechanism remains to be further clarified.

To further verify our hypothesis, we used a protein synthesis inhibitor (CHX), which can inhibit protein synthesis by inhibiting mRNA binding to ribosomes[50]. After CHX administration, we found that occludin content was decreased in the OGD/R + CHX group, but occludin content was still increased in the OGD/R + CHX + GYY group compared with the OGD/R group. This further confirmed that the upregulation of occludin protein by GYY4137 in the early stage after CPR was not achieved by enhancing its mRNA translation process. We know that the relative protein content mainly depends on DNA transcription, RNA translation, protein degradation and other processes. In the present study, the relative expression of occludin mRNA was unchanged, but its

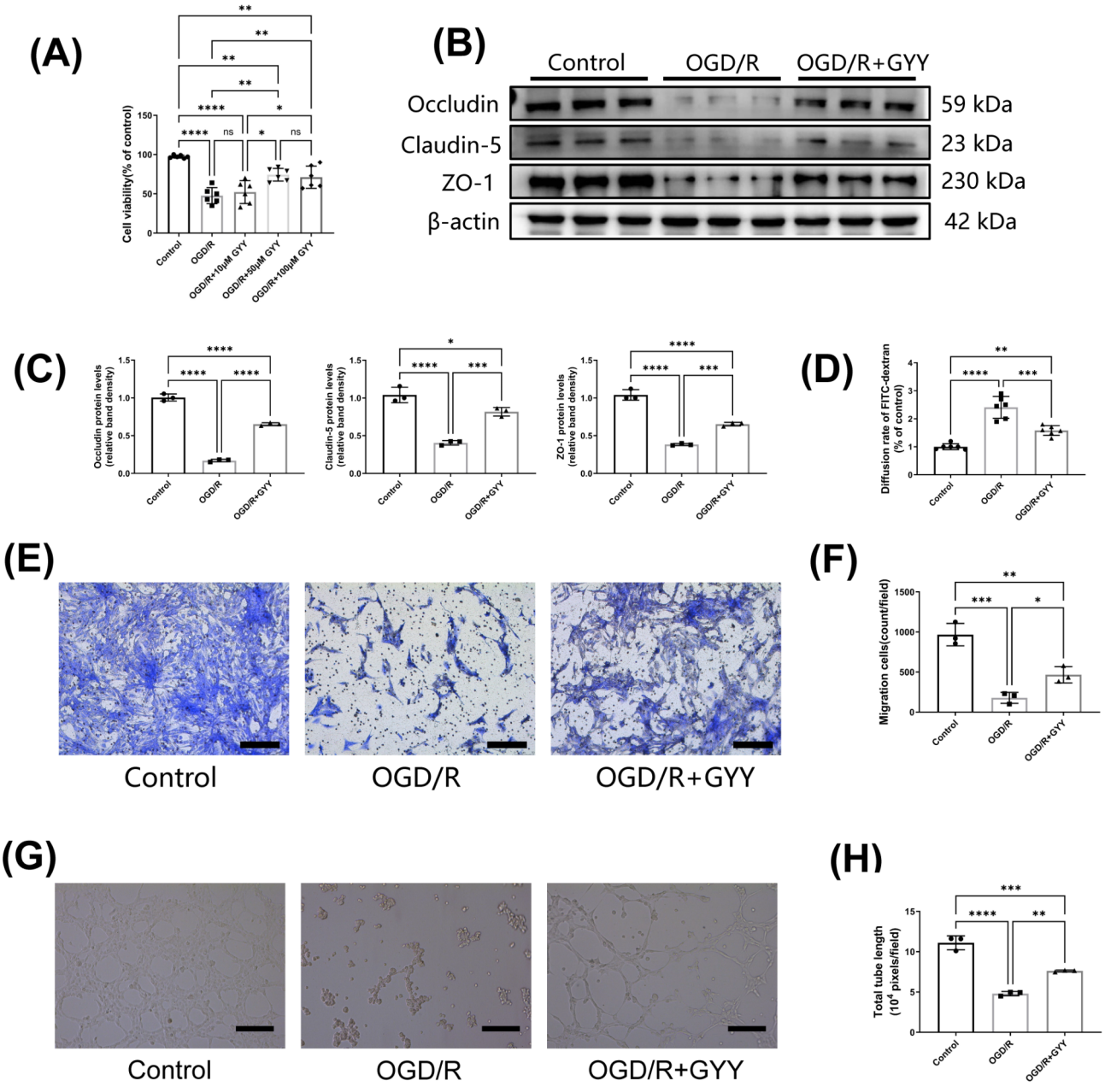

Fig. 3. GYY4137 augmented the function of endothelial cell tight junctions after OGD/R. (**A**) The brain endothelial cell line bEnd.3 was exposed to OGD for 4 h and reperfusion for 12 h. The cell viability of Control, OGD/R, OGD/*R* + 10 μM GYY, OGD/*R* + 50 μM GYY and OGD/*R* + 100 μM GYY groups was examined by CCK-8 assay. (**A**: $P < 0.0001$, F = 20.12). (**B**) Representative immunoblot images and (**C**) quantitation of occludin, claudin-5 and ZO-1 expression in bEnd.3 cells from Control, OGD/R, and OGD/*R* + 50 μM GYY groups. β-actin was used as the protein loading control. The images of western blot data derived from triplicate blots conducted as three independent experiments. (**C**: occludin: $P < 0.0001$, F = 544.3; claudin-5: $P < 0.0001$, F = 63.74; ZO-1: $P < 0.0001$, F = 170.5). (**D**) The diffusion rates of FITC-dextran (40 kDa) in bEnd.3 cells as described in Fig. 3B. (**D**: $P < 0.0001$, F = 46.30). (**E**) Representative images (100×) of transwell migration assay. Cells were stained with 0.1% cresyl violet to visualize migrated cells. Scale bar indicates 100 μm. (**F**) Quantitative analysis of migration cells from the Control, OGD/R, and OGD/R + GYY groups. (**F**: $P = 0.0003$, F = 41.29). (**G**) Representative images (100×) of transwell migration assay and (**H**) quantitative analysis of total tube length from the Control, OGD/R, and OGD/R + GYY groups. Scale bar indicates 100 μm. (**H**: $P < 0.0001$, F = 108.6). The data are the means ± SD. $n \geq 3$. $^*P < 0.05$; $^{**}P < 0.01$; $^{***}P < 0.001$; $^{****}P < 0.0001$.

protein content was significantly increased. Therefore, we speculate that the upregulation of occludin protein by GYY4137 might be achieved by inhibiting its protein degradation.

We further validated this speculation using the proteasome inhibitor MG-132, which inhibits proteasomes involved in ubiquitination degradation[51–53], and the autophagy inhibitor CQ, which inhibits the binding of autophagosomes and lysosomes[54]. As shown in Fig. 5D, the content of occludin protein did not increase after MG-132 treatment but increased after CQ treatment, suggesting that the reduction of occludin content in the early stage after CA/CPR might be mainly mediated through the protein autophagy pathway to enhance its protein degradation, rather than through ubiquitin-proteasome degradation pathway. To further validate this possible regulatory mechanism, we used autophagy enhancer rapamycin, which promotes the binding of autophagosomes and lysosomes[55]. We confirmed that endothelial cells experienced a significant decrease in occludin after OGD/R. Treatment with GYY4137 inhibited the decrease of occludin, accompanied by a decrease in the expression of autophagy-related proteins. In addition, the upregulation of occludin by GYY4137 was reversed after enhancement of autophagy with rapamycin. The above results suggest the increased occludin by GYY4137 might be regulated by inhibiting autophagic degradation pathway. Compared with previous studies, this study provides more insight into the mechanism of BBB injury in the early stage after CA/CPR (illustrated in Supplementary Fig. 3). While CA/CPR caused a reduction in claudin-5 and ZO-1 mRNA expression as well as a corresponding decrease in claudin-5 and ZO-1 protein expression, the decrease in occludin protein did not occur in this manner but rather through increased autophagy-related degradation of occludin. The upregulation of occludin by GYY4137 was also confirmed to exert a protective effect by inhibiting autophagy meditated degradation of occludin.

Although the present study focused on the effects of GYY4137 on the BBB after CA/CPR, it should be noted that H_2S and GYY4137 can exert protective effects on neurons, astrocytes, and microglia in CNS diseases[56–58]. In the model of Alzheimer's disease, GYY4137 was found to preserve hippocampal neurons by slowly releasing H_2S[56]. In addition, GYY4137 has been shown to prevent oxidative stress-induced astrocyte death in studies involving spontaneously hypertensive rats[57]; and in a model of LPS-induced microglial injury, GYY4137 reduced the increase of phosphorylated checkpoint kinase 1 (p-Chk1) and γ-H2AX levels, alleviating neuroinflammation and anxiety-like behavior[58]. These findings suggest that the protective effects of GYY4137 is multifaceted and may involve regulation of neurons, astrocytes, microglia, and other nerve cells. In the present study, we confirmed the protective effect of GYY4137 on the BBB after CA/CPR through in vivo and in vitro experiments, which adds new evidence for further comprehensive understanding the protective effects of GYY4127 and H_2S.

Our study has certain limitations. First, our study used a mouse model, and although mice are physiologically and genetically similar to humans, there are many differences. Therefore, it remains to be investigated whether the protective effects of GYY4137 observed in mice are applicable to humans. Second, the CA/CPR model employed replicates some of the pathophysiologic changes of cardiac arrest in humans but does not include all clinical scenarios. Experimental conditions such as drug dosage and time of administration may differ from clinical practice, which may affect the generalizability of our findings. To enhance the translational potential of our findings, future studies should evaluate the effects of GYY4137 in other animal models, especially those with physiological structures more similar to humans. In addition, further in-depth investigation of the specific molecular mechanisms by which GYY4137 inhibits autophagy and protects the BBB is essential to elucidate its mechanism of action.

Conclusion

In conclusion, our study demonstrated that GYY4137 could exert neuroprotective effects by reducing systemic inflammation and improving BBB dysfunction in the early stage after CA/CPR. GYY4137 can improve BBB function by increasing the content of occludin, which is achieved by inhibiting autophagy meditated occludin degradation rather than promoting its synthesis. These findings broaden the understanding of the molecular mechanisms involved in maintaining BBB function and elucidate the regulatory mechanism of GYY4137 on BBB protection after CA/CPR.

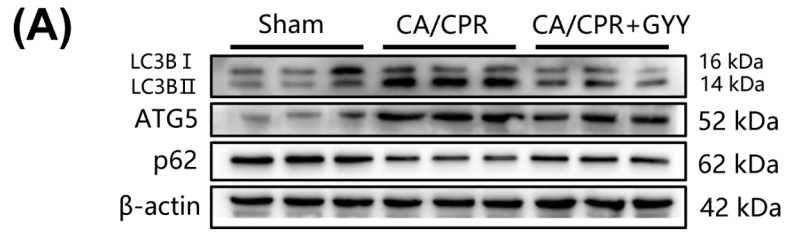
(A)
Sham
CA/CPR
CA/CPR+GYY
LC3B Ⅰ
LC3BⅡ
ATG5
p62
β-actin
16 kDa
14 kDa
52 kDa
62 kDa
42 kDa

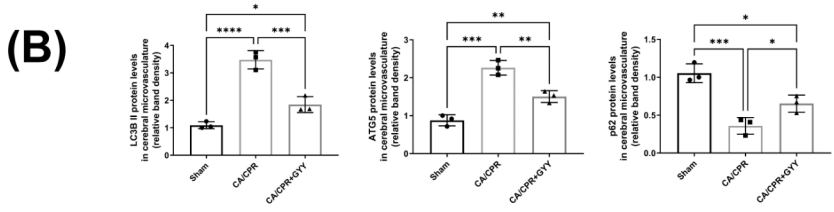
(B)
LC3B II protein levels in cerebral microvasculature (relative band density)
ATG5 protein levels in cerebral microvasculature (relative band density)
p62 protein levels in cerebral microvasculature (relative band density)
Sham
CA/CPR
CA/CPR+GYY

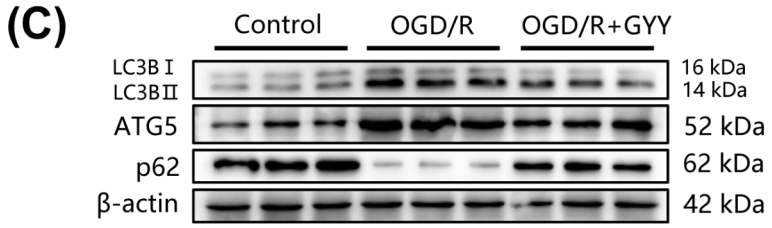
(C)
Control
OGD/R
OGD/R+GYY
LC3B Ⅰ
LC3BⅡ
ATG5
p62
β-actin
16 kDa
14 kDa
52 kDa
62 kDa
42 kDa

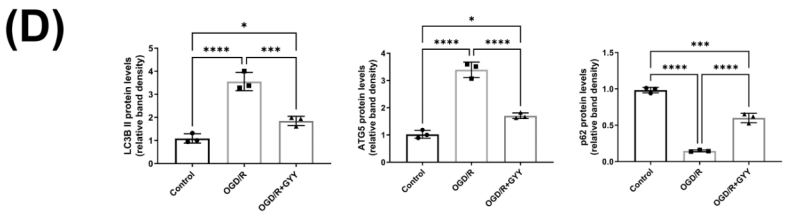
(D)
LC3B II protein levels (relative band density)
ATG5 protein levels (relative band density)
p62 protein levels (relative band density)
Control
OGD/R
OGD/R+GYY

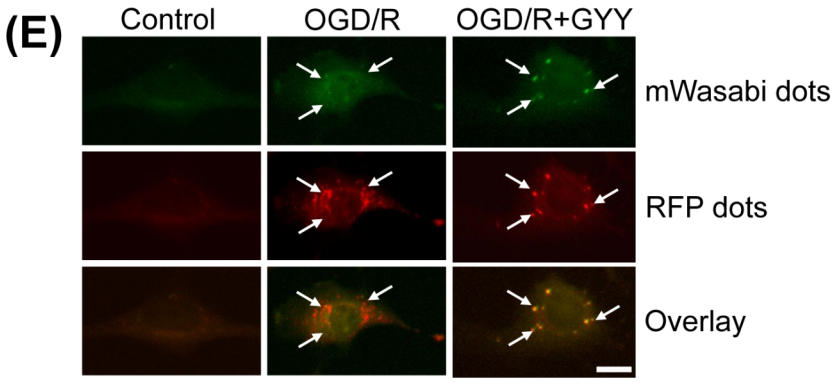
(E)
Control
OGD/R
OGD/R+GYY
mWasabi dots
RFP dots
Overlay

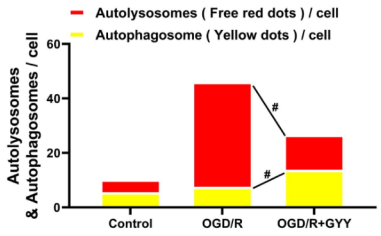
(F)
Autolysosomes (Free red dots) / cell
Autophagosome (Yellow dots) / cell
Autolysosomes & Autophagosomes / cell
Control
OGD/R
OGD/R+GYY

◀**Fig. 4**. GYY4137 inhibited autophagy in BBB endothelial cells in the early stage after resuscitation; and autophagy mediated the regulation of occludin protein content. (**A**) Representative immunoblot images and (**B**) quantitation of LC3B II, ATG5 and p62 in cerebral microvessels of mice in Sham, CA/CPR, CA/CPR + GYY, and CA/CPR + Rapa groups at 24 h after ROSC. β-actin was used as the protein loading control. The images of western blot data derived from triplicate blots conducted as three independent experiments. (**B**: LC3B II: $P < 0.0001$, F = 63.68; ATG5: $P = 0.0002$, F = 52.14; p62: $P = 0.0010$, F = 26.98). (**C**) Representative immunoblot images and (**D**) quantitation of LC3B II, ATG5 and p62 in bEnd.3 cells from Control, OGD/R, and OGD/R + GYY groups. β-actin was used as the protein loading control. The images of western blot data derived from triplicate blots conducted as three independent experiments. (**D**: LC3B II: $P = 0.0001$, F = 60.76; ATG5: $P < 0.0001$, F = 118.6; p62: $P < 0.0001$, F = 269.2). (**E**) The bEnd.3 cells were transfected with flag-tagged RFP-mWasabi-LC3 lentiviral vector in Control, OGD/R, and OGD/R + GYY groups. Representative images of fluorescent LC3 dots are shown. (**F**) Mean number of autophagosomes (dots with both red and green color; i.e., dots with yellow color in merged images) and autolysosomes (dots with only red but not green color; i.e., dots with red color in merged images) per cell. Scale bar indicates 20 μm. (**F**: red: $P < 0.0001$, F = 186.4; yellow: $P < 0.0001$, F = 28.39). The data are the means ± SD. $n \geq 3$. $^{\#}P < 0.05$ versus OGD/R. $^{*}P < 0.05$; $^{**}P < 0.01$; $^{***}P < 0.001$; $^{****}P < 0.0001$.

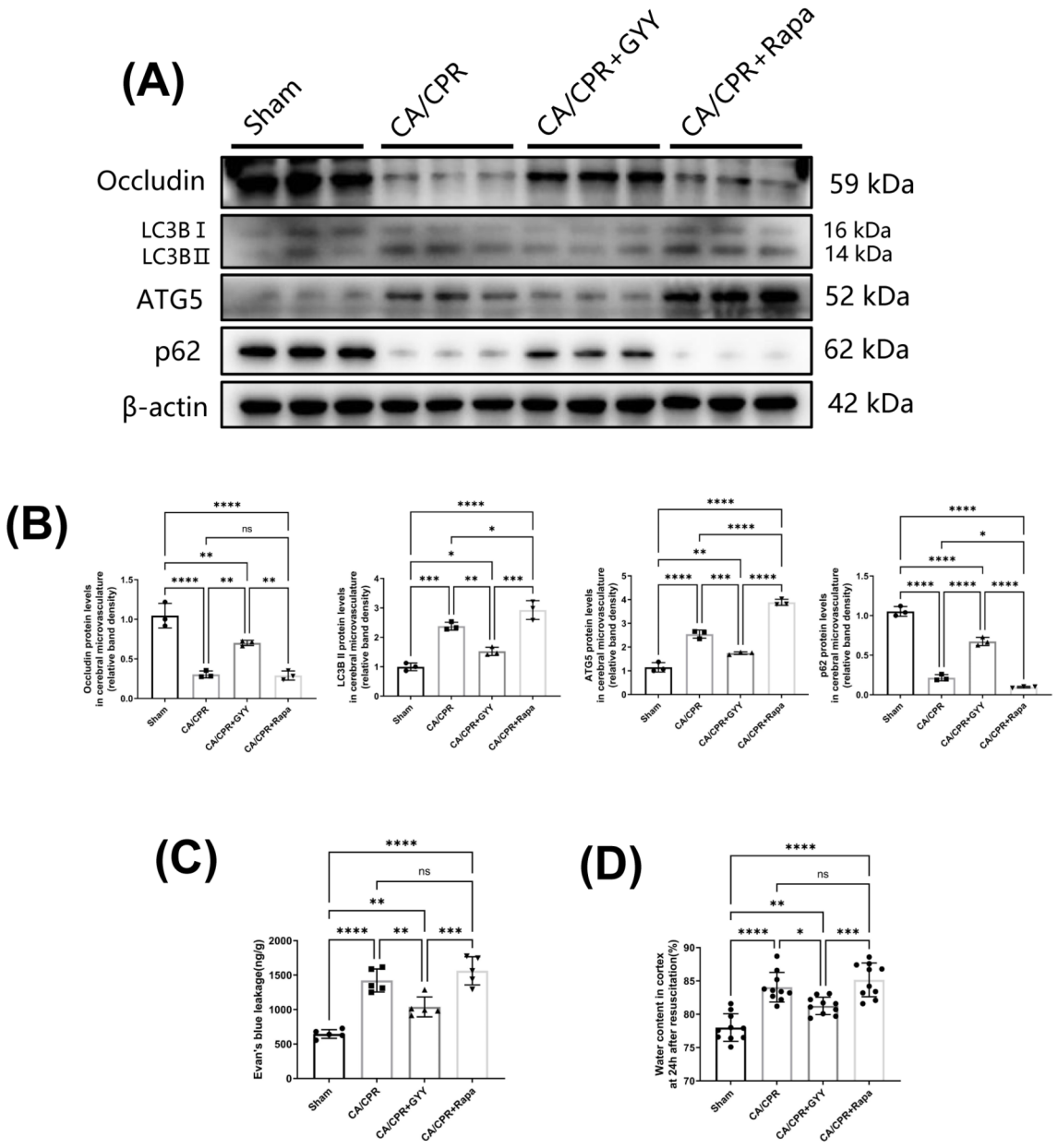

Fig. 5. Rapamycin did not further exacerbate the decrease of occludin protein and BBB damage in mice after CA/CPR. (**A**) Representative immunoblot images and (**B**) quantitation of occludin, LC3B II, ATG5 and p62 in cerebral microvessels of mice in Sham, CA/CPR, CA/CPR + GYY, and CA/CPR + Rapa groups at 24 h after ROSC. β-actin was used as the protein loading control. The images of western blot data derived from triplicate blots conducted as three independent experiments. (**B**: occludin: $P < 0.0001$, F = 51.56; LC3B II: $P < 0.0001$, F = 56.67; ATG5: $P < 0.0001$, F = 189.9; p62: $P < 0.0001$, F = 285.6). (**C**) BBB permeability evaluated using EB at 24 h after ROSC. (**C**: $P < 0.0001$, F = 35.97). (**D**) Brain water content of mice in Sham, CA/CPR, CA/CPR + GYY, and CA + Rapa groups at 24 h after ROSC. (**D**: $P < 0.0001$, F = 23.62). The data are the means ± SD. $n \geq 3$. $^{*}P < 0.05$; $^{**}P < 0.01$; $^{***}P < 0.001$; $^{****}P < 0.0001$.

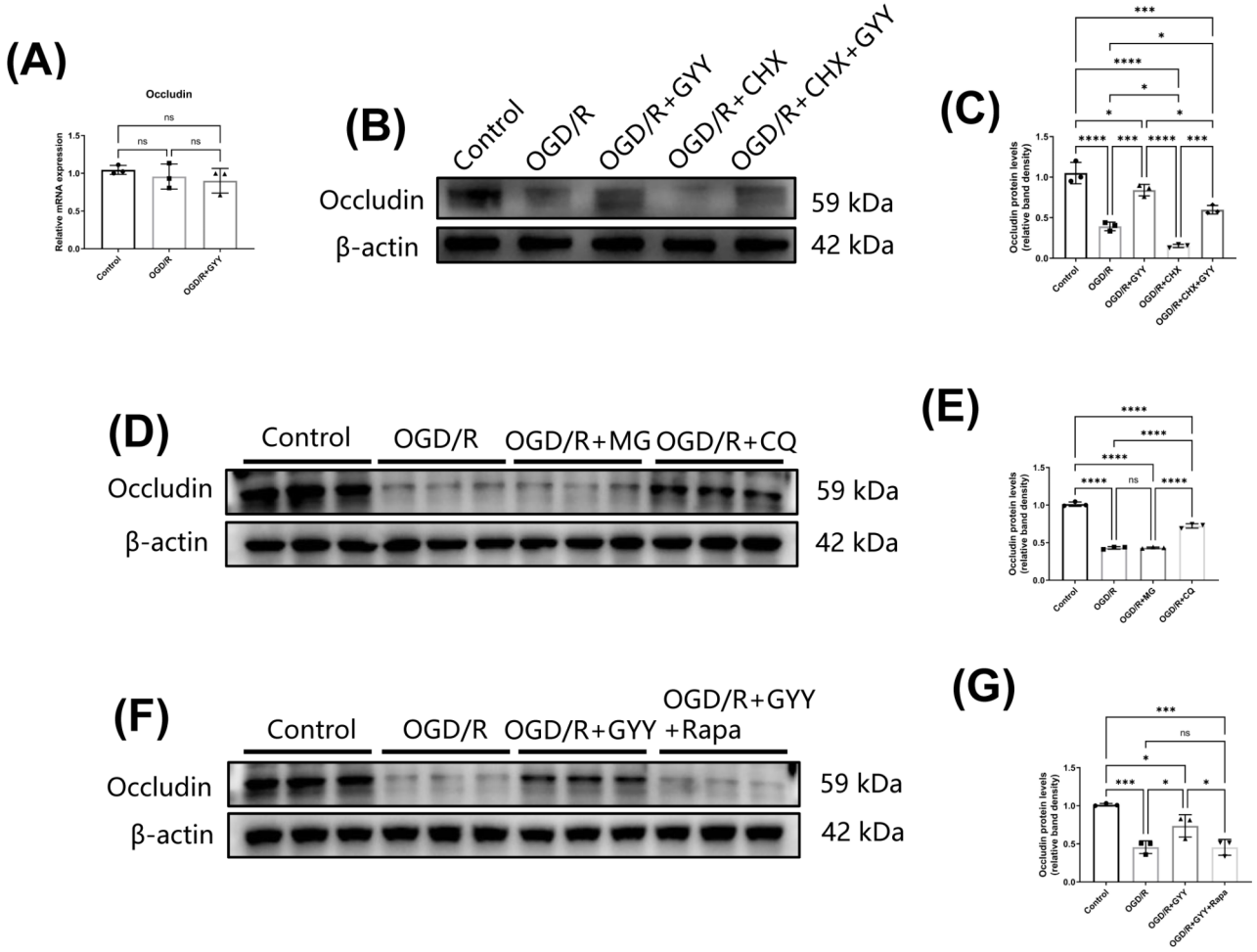

Fig. 6. Autophagy mediated protein degradation is the predominant mechanism behind the reduction of occludin following OGD/R. (**A**) Relative mRNA expression of occludin in bEnd.3 cells from Control, OGD/R, and OGD/R + GYY groups. (**A**: $P = 0.4837$, F = 0.8216). (**B**) Representative immunoblot images and (**C**) quantitation of occludin in bEnd.3 cells from Control, OGD/R, OGD/R + GYY, OGD/R + CHX, and OGD/R + CHX + GYY groups. (**C**: $P < 0.0001$ F = 66.22). (**D**) Representative immunoblot images and (**E**) quantitation of occludin in bEnd.3 cells from Control, OGD/R, OGD/R + MG, and OGD/R + CQ groups. The images of western blot data derived from triplicate blots conducted as three independent experiments. (**E**: $P < 0.0001$, F = 441.8). (**F**) Representative immunoblot images and (**G**) quantitation of occludin in bEnd.3 cells from Control, OGD/R, OGD/R + GYY, and OGD/R + GYY + Rapa groups. The images of western blot data derived from triplicate blots conducted as three independent experiments. (**G**: $P = 0.0003$, F = 21.59). β-actin was used as the protein loading control. The data are the means ± SD. $n \geq 3$. $^{*}P < 0.05$; $^{**}P < 0.01$; $^{***}P < 0.001$; $^{****}P < 0.0001$.

Data availability

Data is provided within the manuscript or supplementary information files.

Received: 16 October 2024; Accepted: 30 December 2024
Published online: 06 January 2025

References

1. Hayman, E. G. et al. Cerebral edema after cardiopulmonary resuscitation: A therapeutic target following Cardiac arrest? *Neurocrit Care*. **28**, 276–287 (2018).
2. Zhu, J. et al. Glycocalyx degradation leads to blood-brain barrier dysfunction and brain edema after asphyxia cardiac arrest in rats. *J. Cereb. Blood Flow. Metab.* **38**, 1979–1992 (2018).
3. Schluep, M. et al. One-year survival after in-hospital cardiac arrest: A systematic review and meta-analysis. *Resuscitation* **132**, 90–100 (2018).
4. Flierl, M. A. et al. Inhibition of complement C5a prevents breakdown of the blood-brain barrier and pituitary dysfunction in experimental sepsis. *Crit. Care*. **13**, R12 (2009).
5. Chen, J. et al. Flufenamic acid improves survival and neurologic outcome after successful cardiopulmonary resuscitation in mice. *J. Neuroinflammation*. **19**, 214 (2022).
6. Li, H. et al. Hydrogen sulfide decreases blood-brain barrier damage via regulating protein kinase C and tight Junction after Cardiac arrest in rats. *Cell. Physiol. Biochem.* **47**, 994–1006 (2018).
7. Pan, J. J. et al. M2 microglial extracellular vesicles attenuated blood-brain barrier disruption via MiR-23a-5p in cerebral ischemic mice. *Aging Dis.* Aug 18. (2023).
8. Li, X. et al. Cerium oxide nanoparticles with antioxidative neurorestoration for ischemic stroke. *Biomaterials* **291**, 121904 (2022).
9. Cao, X. et al. Therapeutic potential of sulfur-containing natural products in inflammatory diseases. *Pharmacol. Ther.* **216**, 107687 (2020).
10. Jia, J., Li, J. & Cheng, J. H_2S-based therapies for ischaemic stroke: Opportunities and challenges. *Stroke Vasc Neurol.* **4**, 63–66 (2019).
11. De Meyer, G. R. et al. Autophagy in vascular disease. *Circ. Res.* **116**, 468–479 (2015).
12. Li, L. et al. Microglia Autophagy mediated by TMEM166 promotes ischemic stroke secondary to carotid artery stenosis. *Aging Dis.* Aug **15**. (2023).
13. Liu, M. et al. Activin a alleviates neuronal injury through inhibiting cGAS-STING-mediated autophagy in mice with ischemic stroke. *J. Cereb. Blood Flow. Metab.* **43**, 736–748 (2023).
14. Zhou, F. et al. HSPB8-Mediated actin filament reorganization by promoting autophagic flux confers resilience to blood-brain barrier (BBB) Injury in an in vitro model of ischemic stroke. *ACS Chem. Neurosci.* **14**, 2868–2875 (2023).
15. Yang, B. et al. Selenium attenuates ischemia/reperfusion injury-induced damage to the blood-brain barrier in hyperglycemia through PI3K/AKT/mTOR pathway-mediated autophagy inhibition. *Int. J. Mol. Med.* **48**, 178 (2021).
16. Gao, S. et al. H_2S attenuates sleep deprivation-induced cognitive impairment by reducing excessive autophagy via hippocampal Sirt-1 in WISTAR RATS. *Neurochem Res.* **46**, 1941–1952 (2021).
17. Yang, T. et al. AP39 inhibits ferroptosis by inhibiting mitochondrial autophagy through the PINK1/parkin pathway to improve myocardial fibrosis with myocardial infarction. *Biomed. Pharmacother.* **165**, 115195 (2023).
18. Feng, J., Li, H. & Wang, S. Hydrogen sulfide alleviates uremic cardiomyopathy by regulating PI3K/PKB/mTOR-mediated overactive autophagy in 5/6 nephrectomy mice. *Front. Pharmacol.* **13**, 1027597 (2022).
19. Latorre, E. et al. Mitochondria-targeted hydrogen sulfide attenuates endothelial senescence by selective induction of splicing factors HNRNPD and SRSF2. *Aging (Albany NY)*. **10**, 1666–1681 (2018).
20. Nin, D. S. et al. Biological effects of Morpholin-4-Ium 4 Methoxyphenyl (Morpholino) Phosphinodithioate and other Phosphorothioate-based hydrogen sulfide donors. *Antioxid. Redox Signal.* **32**, 145–158 (2020).
21. Kilkenny, C. et al. Animal research: Reporting in vivo experiments: the ARRIVE guidelines. *Br. J. Pharmacol.* **160**, 1577–1579 (2010).
22. McGrath, J. C. et al. Guidelines for reporting experiments involving animals: The ARRIVE guidelines. *Br. J. Pharmacol.* **160**, 1573–1576 (2010).
23. Liu, H. et al. Novel modification of potassium chloride induced cardiac arrest model for aged mice. *Aging Dis.* **9**, 31–39 (2018).
24. Ikeda, T. et al. Post-cardiac arrest Sedation promotes Electroencephalographic slow-wave activity and improves survival in a mouse model of Cardiac arrest. *Anesthesiology* **137**, 716–732 (2022).
25. Lourenco, M. V. et al. Exercise-linked FNDC5/irisin rescues synaptic plasticity and memory defects in Alzheimer's models. *Nat. Med.* **25**, 165–175 (2019).
26. Yanagida, K. et al. Size-selective opening of the blood-brain barrier by targeting endothelial sphingosine 1-phosphate receptor 1. *Proc. Natl. Acad. Sci. U S A*. **114**, 4531–4536 (2017).
27. Xiong, W. X. et al. Impaired spatial learning and memory after sevoflurane-nitrous oxide anesthesia in aged rats is associated with down-regulated cAMP/CREB signaling. *PLoS One*. **8**, e79408 (2013).
28. Dzialowski, I. et al. Brain tissue water uptake after middle cerebral artery occlusion assessed with CT. *J. Neuroimaging.* **14**, 42–48 (2004).
29. Geng, Y. et al. Hydrogen sulfide inhalation decreases early blood-brain barrier permeability and brain edema induced by cardiac arrest and resuscitation. *J. Cereb. Blood Flow. Metab.* **35**, 494–500 (2015).
30. Witt, K. A. et al. Hypoxia-inducible factor and nuclear factor kappa-B activation in blood-brain barrier endothelium under hypoxic/reoxygenation stress. *J. Neurochem*. **92**, 203–214 (2005).
31. Bales, K. R. et al. Passive immunotherapy targeting amyloid-β reduces cerebral amyloid angiopathy and improves vascular reactivity. *Brain* **139**, 563–577 (2016).
32. Diaz Sanchez, L. et al. TNF-α-Mediated endothelial cell apoptosis is rescued by Hydrogen Sulfide. *Antioxid. (Basel)*. **12**, 734 (2023).
33. Tian, D. S. et al. FSAP aggravated endothelial dysfunction and neurological deficits in acute ischemic stroke due to large vessel occlusion. *Signal. Transduct. Target. Ther.* **7**, 6 (2022).
34. Buonarati, O. R. et al. CaMKII versus DAPK1 binding to GluN2B in ischemic neuronal cell death after resuscitation from Cardiac arrest. *Cell. Rep.* **30**, 1–8e4 (2020).
35. Banerjee, S. et al. Exacerbating effects of single-dose acute ethanol exposure on neuroinflammation and amelioration by GPR110 (ADGRF1) activation. *J. Neuroinflammation*. **20**, 187 (2023).
36. Patabendige, A. & Janigro, D. The role of the blood-brain barrier during neurological disease and infection. *Biochem. Soc. Trans.* **51**, 613–626 (2023).
37. Bernardo-Castro, S. et al. The evolution of blood-brain barrier permeability changes after stroke and its implications on clinical outcome: A systematic review and meta-analysis. *Int. J. Stroke*. **18**, 783–794 (2023).
38. Lascola, C. D. et al. Blood-brain barrier permeability and cognitive dysfunction after surgery - A pilot study. *J. Clin. Anesth.* **86**, 111059 (2023).
39. Bernardo-Castro, S. et al. Pathophysiology of blood-brain barrier permeability throughout the different stages of ischemic stroke and its implication on Hemorrhagic Transformation and Recovery. *Front. Neurol.* **11**, 594672 (2020).
40. Cui, W. et al. GYY4137 protected the integrity of the blood-brain barrier via activation of the Nrf2/ARE pathway in mice with sepsis. *FASEB J.* **35**, e21710 (2021).
41. Cai, S. et al. Therapeutic hypothermia combined with hydrogen sulfide treatment attenuated early blood-brain barrier disruption and brain Edema Induced by Cardiac arrest and resuscitation in Rat Model. *Neurochem Res.* **48**, 967–979 (2023).
42. Sun, X. et al. Novel controlled and targeted releasing hydrogen sulfide system exerts combinational cerebral and myocardial protection after cardiac arrest. *J. Nanobiotechnol.* **19**, 40 (2021).

43. Lin, J. Y. et al. Hydrogen sulfide improves neural function in rats following cardiopulmonary resuscitation. *Exp. Ther. Med.* **11**, 577–587 (2016).
44. Wang, X. et al. Hydrogen sulfide attenuates disturbed flow-induced vascular remodeling by inhibiting LDHB-mediated autophagic flux. *Redox Biol.* **79**, 103456 (2024).
45. Xu, K. et al. NaHS restores mitochondrial function and inhibits autophagy by activating the PI3K/Akt/mTOR signalling pathway to improve functional recovery after traumatic brain injury. *Chem. Biol. Interact.* **286**, 96–105 (2018).
46. Ge, X. et al. Hydrogen sulfide treatment alleviated ventilator-induced lung injury through regulation of autophagy and endoplasmic reticulum stress. *Int. J. Biol. Sci.* **15** (13), 2872–2884 (2019).
47. Yan, N. et al. Arsenic induces blood–brain barrier disruption and regulates T lymphocyte subpopulation differentiation in the cerebral cortex and hippocampus associated with the Nrf2 pathway in vivo. *Biol. Trace Elem. Res.* **201**, 3981–3993 (2023).
48. Ren, S. et al. Minimally invasive surgery for ICH evacuation combined with deferoxamine treatment increased Perihematomal Claudin-5 and ZO-1 expression levels and decreased BBB permeability in rabbits. *Front. Neurol.* **13**, 835494 (2022).
49. Behera, J., Kelly, K. E. & Tyagi, N. Hydrogen sulfide prevents ethanol-induced ZO-1 CpG promoter hypermethylation-dependent vascular permeability via miR-218/DNMT3a axis. *J. Cell. Physiol.* **236**, 6852–6867 (2021).
50. Burgers, L. D. & Fürst, R. Natural products as drugs and tools for influencing core processes of eukaryotic mRNA translation. *Pharmacol. Res.* **170**, 105535 (2021).
51. Raffeiner, M. et al. Interplay between autophagy and proteasome during protein turnover. *Trends Plant. Sci.* **28**, 698–714 (2023).
52. Li, Y., Li, S. & Wu, H. Ubiquitination-Proteasome System (UPS) and Autophagy Two Main protein degradation machineries in response to cell stress. *Cells* **11**, 851 (2022).
53. Guan, H. et al. Exosomal RNF157 mRNA from prostate cancer cells contributes to M2 macrophage polarization through destabilizing HDAC1. *Front. Oncol.* **12**, 1021270 (2022).
54. Yuan, X. et al. URB597 exerts neuroprotective effects against transient brain ischemia injury in mice by regulating autophagic flux and necroptosis. *Eur. J. Pharmacol.* **957**, 175982 (2023).
55. Yang, J. et al. The circRNA MKLN1 regulates autophagy in the development of diabetic retinopathy. *Biochim. Biophys. Acta Mol. Basis Dis.* **1869**, 166839 (2023).
56. Manakkadan, A. et al. Slow release of hydrogen sulfide in CA1 hippocampal neurons rescues long-term synaptic plasticity and associativity in an Amyloid-β Induced Model of Alzheimer's Disease. *J. Alzheimers Dis.* **101**, 913–921 (2024).
57. Juman, S. et al. Reduced production of Hydrogen Sulfide and Sulfane Sulfur due to low cystathionine β-Synthase levels in brain astrocytes of stroke-prone spontaneously hypertensive rats. *Biol. Pharm. Bull.* **39**, 1932–1938 (2016).
58. Shentu, Y. et al. Hydrogen sulfide ameliorates lipopolysaccharide-induced anxiety-like behavior by inhibiting checkpoint kinase 1 activation in the hippocampus of mice. *Exp. Neurol.* **371**, 114586 (2024).

Author contributions

PYD and BZ designed the study. PYD, XYL, YHB, and WYF performed the experiments. PYD, ZHJ, XQZ, and GHH performed the data analysis and interpretation. PYD wrote the manuscript. BZ, DA, and ZBW reviewed and revised the manuscript for final approval. All authors discussed the results and commented on the manuscript. All authors contributed to the article and approved the submitted version.

Funding

This study was supported by the National Natural Science Foundation of China (8207080606).

Competing interests

The authors declare no competing interests.

Ethics approval and consent to participate

The study protocol was approved by the Institutional Animal Care and Use Committee of Harbin Medical University (Heilongjiang, China).

Additional information

Supplementary Information The online version contains supplementary material available at https://doi.org/10.1038/s41598-024-84948-2.

Correspondence and requests for materials should be addressed to B.Z.